The Journal of Physiology

Molecular determinants underlying volume-regulated anion channel subunit-dependent oxidation sensitivity

Sara Bertelli[1,2,3], Paolo Zuccolini[1], Paola Gavazzo[1] and Michael Pusch[1]

[1] *Istituto di Biofisica, Consiglio Nazionale delle Ricerche, Genova, Italy*
[2] *Scuola Internazionale Superiore di Studi Avanzati (SISSA), Trieste, Italy*
[3] *Molecular Neuroscience and Biophysics, Leibniz-Forschungsinstitut für Molekulare Pharmakologie, Berlin, Germany*

Handling Editors: David Wyllie & Rajini Rao

The peer review history is available in the Supporting information section of this article (https://doi.org/10.1113/JP283321#support-information-section).

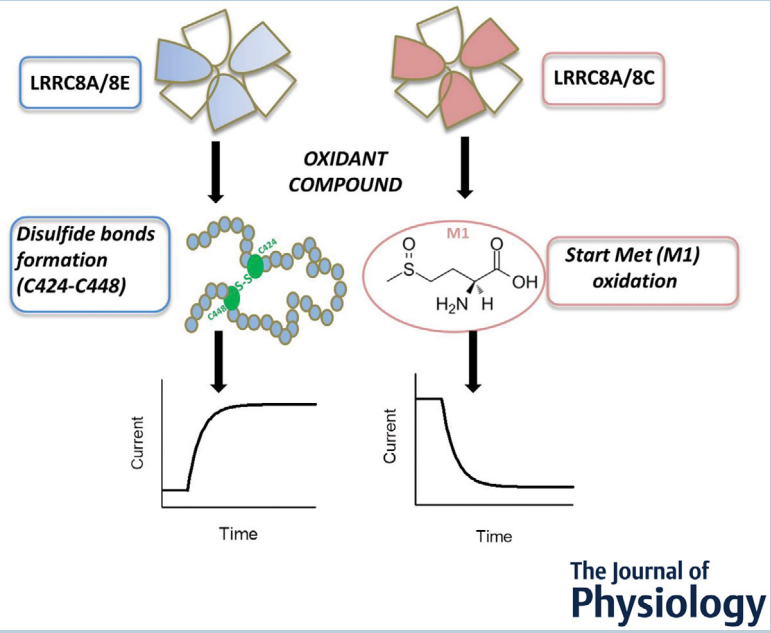

Abstract The volume-regulated anion channel (VRAC) is formed by LRRC8 subunits. Besides their role in the maintenance of cell homeostasis, VRACs are critically involved in oxidative stress mechanisms: reactive oxygen species directly modulate VRACs in a subunit-dependent manner. It was reported that LRRC8A–LRRC8E heteromeric channels are activated by oxidation, whereas LRRC8A–LRRC8C heteromers are inhibited. Here we adopted chimeric- as well as

Sara Bertelli received her masters degree in Medical and Pharmaceutical Biotechnology from the University of Genoa, Italy in 2016 and her PhD in from the SISSA (Scuola Internazionale di Studi Superiori Avanzati) in collaboration with C.N.R. Biophysics Institute of Genova in 2021. Currently she is a postdoc in the lab of Andrew Plested at the Free University of Berlin. Her interests are focused on ion channels ranging from voltage-gated sodium channels to volume-regulated anion channels and glutamate receptors.

DOI: 10.1113/JP283321

concatemeric-based strategies to identify residues responsible for the divergent effect of oxidants. We identified two cysteines in the first two leucine rich repeats of LRRC8E, C424 and C448, as the targets of oxidation. Oxidation likely results in the formation of a disulfide bond between the two cysteines, which in turn induces a conformational change leading to channel activation. Additionally, we found that LRRC8C inhibition is caused by oxidation of the first methionine. We thus identified crucial molecular elements involved in channel activation, which are conceivably relevant in determining physiological ROS effects.

(Received 12 May 2022; accepted after revision 15 July 2022; first published online 21 July 2022)
Corresponding author M. Pusch: Via de Marini 6, Genoa I-16149, Italy. Email: michael.pusch@ibf.cnr.it

Abstract figure legend Volume-regulated anion channels (VRACs) are heteromers composed of LRRC8A–8E subunits and are modulated by oxidative stress in a subunit-dependent manner. Oxidation of VRACs containing 8A and 8E subunits leads to disulfide bond formation between two cysteine residues of 8E located in the leucine rich domain (Cys 424 and 448) and a consequent activation of the channels (left panel). Conversely, application of oxidizing reagents to VRACs composed of 8A and 8C subunits oxidizes the start methionine of the 8C subunit and inhibits the current of pre-activated 8A–8C heteromers (right panel).

Key points

- Volume-regulated anion channels (VRACs) are heterohexameric complexes composed of an essential LRRC8A subunit and a variable number of LRRC8B–E subunits.
- VRACs are directly regulated by oxidation, with LRRC8A–LRRC8E heteromers being potentiated and LRRC8A–LRRC8C heteromers being inhibited by oxidation.
- We identified two LRRC8E specific intracellular cysteines that form a disulfide bond upon oxidation leading to LRRC8A–LRRC8E potentiation.
- Inhibition of LRRC8A–LRRC8C heteromers is mediated by the oxidation of the start methionine, being additionally dependent on the identity of the LRR domain.
- Besides providing physiological insights concerning the outcome of reactive oxygen species modulation, the results point to key structural elements involved in VRAC activation.

Introduction

Cell volume regulation is critical for animal cell survival. To counteract the osmotic challenges arising from physiological processes or pathological states, cells evolved mechanisms aimed at maintaining volume, which must be tightly regulated to ensure their integrity and functionality. These processes are called regulatory volume decrease and regulatory volume increase (Jentsch, 2016). Ubiquitously expressed volume-regulated anion channels (VRACs) play the foremost role in regulatory volume decrease, mediating the swelling-induced extrusion of chloride and organic osmolytes that subsequently drives water efflux through the cell. After their first description in T lymphocytes and intestinal cells (Cahalan & Lewis, 1988; Hazama & Okada, 1988), the molecular identity of the channels remained a mystery for decades, precluding structure–function analyses as well as deeper investigations on relevant triggers leading to channel activation upon cell swelling. It was only in 2014 that two groups independently discovered that the leucine rich repeat-containing protein 8A (LRRC8A) is an essential component of VRACs (Qiu et al., 2014; Voss et al., 2014), and four closely related homologues (LRRC8B to -E) are complementary VRAC subunits (Voss et al., 2014), which differentially associate to give rise to functional heteromers. This finding laid the groundwork for obtaining cryo-EM structures of homomeric LRRC8A and LRRC8D complexes, which confirmed the previously predicted topology and the hexameric nature of the channel (Abascal & Zardoya, 2012; Deneka et al., 2018; Kasuya et al., 2018; Kefauver et al., 2018; Kern et al., 2019; Nakamura et al., 2020).

However, little is known about the relevant VRAC stoichiometry, and the high variability of the expression patterns observed in different cell lines suggests that subunit composition is modified to meet physiological demand (Bertelli et al., 2021; Jentsch, 2016; Okada et al., 2019; Stauber, 2015; Strange et al., 2019). In line with this hypothesis, emerging evidence of subunit-dependent properties arose. For example, LRRC8D-containing heteromers facilitate the permeation of large osmolytes (Gaitán-Peñas et al., 2016; Lutter et al., 2017) and

also allow uptake of the antibiotic blasticidin-S (Lee et al., 2014) and chemotherapeutic drugs (Gradogna, Gaitan-Penas et al., 2017; Planells-Cases et al., 2015). LRRC8A–LRRC8E-containing VRACs were recently reported to be the main channels responsible of cGAMP and cyclic dinucleotide transport, contributing to antiviral defence (Zhou et al., 2020).

Notably, LRRC8 heteromeric channels are differentially regulated by oxidation depending on subunit composition (Gradogna, Gavazzo et al., 2017). The role of reactive oxygen species (ROS) in VRAC activity has been extensively studied. Several works reported that hydrogen peroxide (H_2O_2) can directly elicit VRAC currents even in the absence of hypotonic stimulation (Browe & Baumgarten, 2004; Shimizu et al., 2004; Varela et al., 2004, 2007). On the other hand, VRAC activation itself impacts on the oxidation status, probably by the release of reduced glutathione (Friard et al., 2019). Comprehension of the mutual relation between ROS and VRACs is fundamental to elucidating important processes, like apoptotic volume decrease or oxidative stress, in which VRACs are involved. An important question is whether LRRC8 proteins are directly or indirectly affected by oxidation. Gradogna, Gavazzo et al. (2017) found that LRRC8A–LRRC8C and LRRC8A–LRRC8D heteromers are inhibited by chloramine-T (Chl-T) oxidation, whereas LRRC8A–LRRC8E heteromers are dramatically activated by Chl-T and *tert*-butyl hydroperoxide (TBHP)-mediated oxidation (Gradogna, Gavazzo et al., 2017). In addition, exploitation of membrane-permeant and -impermeant cysteine-modifying reagents showed that oxidation of intracellular residues, most likely cysteines or methionine, is responsible for the effects.

Here, we use a chimeric strategy and point mutations to identify residues responsible for the divergent effects of ROS in LRRC8A/8C compared to LRRC8A/8E heteromers in oxidation-mediated VRAC modulation. This led us to discover two cysteine residues in the first two leucine rich repeats (LRR 1 and 2) of LRRC8E (C424 and C448) as the target of Chl-T and TBHP oxidation. Both cysteines are essential to elicit the strong potentiation of VRAC activity upon Chl-T or TBHP application. This suggests that ROS might cause the formation of a disulfide bond between the two cysteines thus inducing conformational rearrangements of the leucine-rich repeat domains (LRRDs), which, in turn, leads to channel activation. Interestingly, the design of a concatemeric construct in which LRRC8A was fused to LRCC8C with an intervening self-cleavable peptide, which allowed the mutation of the start methionine of LRCC8C to leucine, revealed that the oxidation of the first methionine (M1) underlies inhibition of LRCC8C-containing heteromers by Chl-T. To simplify nomenclature, in the following, we will denote LRRC8A subunits as '8A' and likewise for the other homologues.

Methods

Molecular cloning

For heterologous expression in *Xenopus* oocytes, we used human LRRC8A–E cloned in the pCSDest vector as described before (Gaitán-Peñas et al., 2016). The chimeras and sub-chimeras of LRRC8E/C-mCh were all generated by standard cloning strategies. To substitute the first obligatory methionine residue (M1) in the background of 8C, we exploited the T2A linker technology (Tang et al., 2009) that allows generation of polycistronic constructs by expressing more genes under a single ORF. We generated LRRC8A-VFP-T2A-LRRC8C-mCh, LRRC8A-VFP-T2A-LRRC8C$_{M1L}$-mCh, LRRC8A-VFP-T2A-LRRC8C$_{I431C-K455C}$-mCh and LRRC8A-VFP-T2A-LRRC8C$_{M1L-I431C-K455C}$-mCh constructs. For the sake of simplicity, we will refer to single LRRC8 subunits in short as 8A, 8C and 8E. Heteromers arising from co-expression of single subunits are defined as 8A/8E or 8A/8C, while the T2A concatemer constructs are referred as 8A–8C(M), 8A–8C-(L), 8A–8C(MCC) and 8A- 8C(LCC), respectively. For all experiments with oocytes, in plasmids (cloned in pCSDest) containing LRRC8 cDNA the subunits are C-terminally fused with venus fluorescent protein (VFP) (LRRC8A) or mCherry (mCh) (LRRC8E/LRRC8C). For simplicity, these are denoted as 8A, 8E, … Constructs used for HEK cell transfection (cloned in PEGFP-N1) are either C-terminally tagged or not as explicitly indicated in the text for each experiment (for example, 8A C-terminally tagged by the cerulean fluorescent protein is denoted as 8A-cer, while the untagged subunit is simply denoted as 8A). As established previously (Voss et al., 2014) tagging of one subunit is sufficient to generate a certain degree of basal activity and allows identification of cells that express functional VRACs in the plasma membrane. In particular 8A expressed alone is not properly targeted to the plasma membrane (Voss et al., 2014). Therefore, some experiments were conducted with only one tagged subunit.

Two-electrode voltage clamp

Xenopus oocytes were handled and injected as described (Gaitán-Peñas et al., 2016; Traverso et al., 2006). Oxidizing reagents (1 mM) were freshly added (Chl-T and TBHP). Holding potential was kept at −30 mV. The voltage and time dependence of currents were assayed with a current–voltage (*I–V*) protocol consisting in the application of voltage steps of 3000 ms ranging from −100 to 60 mV in 40 mV increments. To determine the effects of oxidizing agents, 200 ms pulses to 60 mV were applied every 5 s and currents were averaged over the pulse period and plotted as a function of time. In

all figures, capacitive transients are blanked for clarity. For currents larger than 10 μA, series resistance was measured by short current pulses in current clamp configuration and compensated as follows: for the voltage clamp protocols, the effective command voltage, V_{eff}, was adjusted offline according to the calculated series resistance error by $V_{eff} = V_{command} - I \times R_s$, where I is the measured current. The current response at 60 mV was then corrected assuming a linear current–voltage relationship and the measured reversal potential. For constructs that display a relatively small expression (i.e. most concatemers), the estimate of the initial current level, and in case of inhibition, also the final current level, are affected by possible 'leak'/endogenous unrelated current components. The most important criterion for including/rejecting recordings was the stability of the baseline, which is that currents remained stable before application of oxidants. All chemicals were purchased from Sigma-Aldrich (St Louis, MO, USA).

Cell culture

HEK-5X-KO *lrrc8*$^{-/-}$ cells (for short: LRRC8(−/−)HEK) used for patch clamp recordings were knock-out for all five genes encoding LRRC8 subunits (Lutter et al., 2017) and were kindly provided by Thomas Jentsch (Berlin). LRRC8(−/−)HEK were cultured in Dulbecco's modified Eagle's medium (Pan Biotech, Aidenbach, Germany) supplemented with 10% fetal bovine serum, 1% penicillin–streptomycin and 1% glutamine and maintained at 37°C in a 5% CO_2, 100% humidity atmosphere. Cells were grown on plastic tissue culture dishes and split every 3−4 days.

Transfection was performed as described (Ferrera et al., 2021). The amount of cDNA used varied according to the experiments. Currents were recorded 24−36 h after transfection.

Patch-clamp recording

Whole-cell voltage clamp experiments were performed as described (Ferrera et al., 2021). Series resistance (R_S) assessed during whole cell recordings was between 2 and 8 MΩ and usually not corrected for, and cell capacitance (C_m) was 10−40 pF (mean ± SD, $R_S = 5.1 \pm 2.8$ MΩ, $C_m = 22.8 \pm 5.3$ pF). The holding potential was −25 mV.

The standard *I–V* for stimulation consisted of 500 ms voltage steps ranging from −80 to 120 mV in 20 mV increments. Current response to the various stimuli was monitored using the 'time course protocol', which consisted of successive steps of 50 ms pulses to −75, −25, 0, 25 and 75 mV every 5 s. These steps allowed us to verify the absence of a significant leak conductance because the expected reversal potential is −25 mV and VRAC currents are slightly outwardly rectifying under the ionic conditions used.

All experiments that included the external application of a molecular compound were performed only after the stability of the baseline was reached (time-course control protocols usually lasting 2 min). All Chl-T applications were done in isotonic solutions.

Data were analysed with the program Ana (available at http://users.ge.ibf.cnr.it/pusch/programs-mik.htm) and Sigma Plot (Systat Software, Inc., San Jose, CA, USA).

Solutions with different ionic composition and osmolarity were used for experiments as follows. The standard extracellular isotonic solution contained (in mM): 145 NaCl, 6 KCl, 1.5 $CaCl_2$, 1 $MgCl_2$, 10 Hepes, 10 glucose (pH 7.4, 310 mOsm). Hypotonic solution contained (in mM): 105 NaCl, 6 CsCl, 1.5 $CaCl_2$, 1 $MgCl_2$, 10 Hepes, 10 glucose (pH7.4, 230 mOsm). Experiments to monitor VRAC activation under oxidative conditions were performed by addition of fresh Chl-T (500 μM or 1 mM) to the respective extracellular solutions. The standard pipette solution to monitor VRAC activation upon hypotonic perfusion contained (in mM): 100 potassium gluconate, 40 CsCl, 2 $MgCl_2$, 1.9 $CaCl_2$, 5 EGTA-NMDG, 1 Na_2ATP, and 10 Hepes-NMDG, pH 7.3 (290 mOsm). The free Ca^{2+} concentration in this solution was calculated to be ∼80 nM.

In some experiments, the non-specific VRAC inhibitor carbenoxolone (CBX) was applied at 100 μM. The compound was directly dissolved in the extracellular solution.

For the identification of cells transfected with untagged constructs, a plasmid encoding the CD8 antigen was co-transfected. The transfected cells were identified by microbeads coated with anti-CD8 antibodies (Dynabeads M-450 CD 8; Thermo Fisher Scientific, Waltham, MA, USA) as described (Jurman et al., 1994).

For analysis, current amplitudes during time course protocols were determined as the mean current acquired during the 60 mV (oocytes) or 75 mV (HEK cells) step, measured after approximately 10 ms of the voltage change to exclude artifacts from capacitive currents.

Image acquisition

Fluorescence was evoked and measured using a Till monochromator based imaging system with an Imago cooled CCD camera mounted on an Axiovert Zeiss microscope and controlled by TillVision software (Till photonics, München, Germany). Fluorescence was excited at 480/560 nm and acquired using a double band emission filter.

Statistics and reproducibility

Data parameters were expressed as means ± SD of n independent oocytes or HEK cells. Statistical significance

($^{*}P < 0.05$, $^{**}P < 0.01$, $^{***}P < 0.001$) was determined using Student's paired *t*-test or a one-way ANOVA, as appropriate (GraphPad Prism, GraphPad Software Inc., San Diego, CA, USA). When a statistically significant difference was determined with ANOVA, a *post hoc* Tukey's test, unpaired *t*-test with Welch's correction, or unpaired *t*-test with Mann–Whitney's correction was used to evaluate which data groups showed significant differences. *P*-values <0.05 were considered significant.

Construction of homology models

We used the 'User template' mode of the Swiss Homology model server (https://swissmodel.expasy.org/interactive#structure) to create various homology models of heteromeric human LRRC8 channels of putative stoichiometry. All modelling was based on the pdb entry 6G9O (Deneka et al., 2018) of homomeric LRRC8A. In order to constrain the composition of a hexameric protein we artificially created a pdb file in which all six chains of the LRRC8A of the 6G9O entry were combined to a single chain, used as template. To create a model of a hexamer with 8A–8E–8A–8E–8A–8E composition we concatenated the sequences of 8A and 8E subunits accordingly in a single file using this as the target sequence for Swiss Model. The resulting homology model pdb file was then again split into different chains for the various subunits. In this way, we constructed a model corresponding to the following subunits stoichiometry: A–E–A–E–A–E, E–A–E–A–E–A (note that these two are not equivalent due to the symmetry breaking at the level of the LRRC domains; Deneka et al., 2018) and A–C–A–C–A–C, C–A–C–A–C–A.

Results

Chimeras of 8E and 8C

Previous results obtained in oocytes suggested that the effects observed upon Chl-T application on 8A/8C and 8A/8E heteromers are mediated by the oxidation of intracellularly localized residues (Gaitán-Peñas et al., 2016). We first intended to determine which domain might be the target of Chl-T among the various cytosolic regions of LRRC8 subunits. In addition to the LRRD, these include the N-terminus, the intracellular loop between TM2 and TM3 (IL1), and the linker connecting the C-terminal end of TM4 with the first LRR.

We employed *Xenopus* oocytes as a heterologous expression system, by injecting LRRC8 subunits containing a fluorescent tag at the C-terminus. All experiments were performed by co-injecting 8A together with 8E or 8C, since 8A expression is essential to give rise to functional channels (Voss et al., 2014). Expression of these constructs results in partially constitutively active channels, that are ideal for monitoring activation or inactivation of current, without the need of pre-stimulation by osmotic stress (Gaitán-Peñas et al., 2016, 2018). Importantly, these channels can be further stimulated by hypotonicity, demonstrating that the machinery of volume sensitivity is fully active in the tagged constructs (Gaitán-Peñas et al., 2016). Using these constructs does not allow addressing the question of whether oxidation of 8A/8E heteromers activates the channels '*de novo*'. However, experiments with untagged subunits clearly favour the idea that this is the case (see below).

We hypothesized that the LRRDs might be the relevant target of Chl-T oxidation. To test this possibility, we swapped the LRRDs between 8C and 8E using a chimeric approach. Interestingly, LRRD exchange resulted in a corresponding interchange of the respective oxidation sensitivity: the chimera 8A/8C(LRRD,8E) (for short CE) displayed a significant potentiation of the currents of 2- to 4-fold, while 8A/8E(LRRD,8C) (for short EC) currents were inhibited by about 50% (Fig. 1*A*). This finding confirmed the intracellular localization of the relevant residues underlying oxidation sensitivity and suggested LRRD as a possible target.

Next, we designed successive chimeras to further narrow down putative regions responsible for oxidant modulation. We first focused on the screening of residues responsible for current potentiation of 8A/8E heteromers upon application of Chl-T or *tert*-butyl hydroperoxide (TBHP), another organic oxidizing agent which was previously shown to potentiate 8A/8E complexes, but which has no effect on 8A/8C heteromers (Fig. 1*B*) (Gradogna, Gavazzo et al., 2017). Chimeras were designed by dividing the LRRD into four pieces following the logic of the bisection method. This procedure resulted in the chimeras Eec, Ece, E$\varepsilon\chi$e and E$\chi\varepsilon$E (see legend of Fig. 1). Investigation of successively generated sub-chimeras showed that activation of 8A/8E heteromers is most likely mediated by oxidation of residues within leucine rich repeats 1–4 (LRR 1−4), in that only chimeras that contained LRR 1−4 of 8E behaved similarly to 8A/8E upon Chl-T and TBHP oxidation (Fig. 1*B*–*D*). As can be noticed from the mean fold increase (Fig. 1*D*), the logic of the bisection method turned out to be useful to distinguish between different phenotypes and accordingly unmask potential regions as the target of oxidation. However, even though both the time course and the mean fold increase of the E$\varepsilon\chi$e chimera support our first conclusion that the LRR 1−4 region indeed contains the essential reactive residues underlying the 8E activatory phenotype upon Chl-T application, results for the E$\chi\varepsilon$e chimera were inconclusive in that it exhibited a complex biphasic behaviour difficult to interpret (Fig. 1*C* and *D*). Overall, the chimeric strategy was not conclusive

regarding the inhibitory effect of Chl-T on 8A/8C heteromers.

Point mutations reveal C424 and C448 as targets in 8E

As previously reported, the use of the membrane-permeant cysteine reactive compound methyl methanethiosulfonate prevented the potentiation by Chl-T, suggesting cysteine residues as the oxidation target of 8E (Gradogna, Gavazzo et al., 2017). Thus, the exclusion of cysteines external to LRR 1–4 from the list of potential mediators of Chl-T effects on 8A/8E left as candidates only three residues: C424, C448 and C493 (Fig. 1*E*). We first generated a triple mutant in the background of 8E where cysteines 424, 448 and 493 were mutated to phenylalanine, serine and leucine, respectively (C424F,

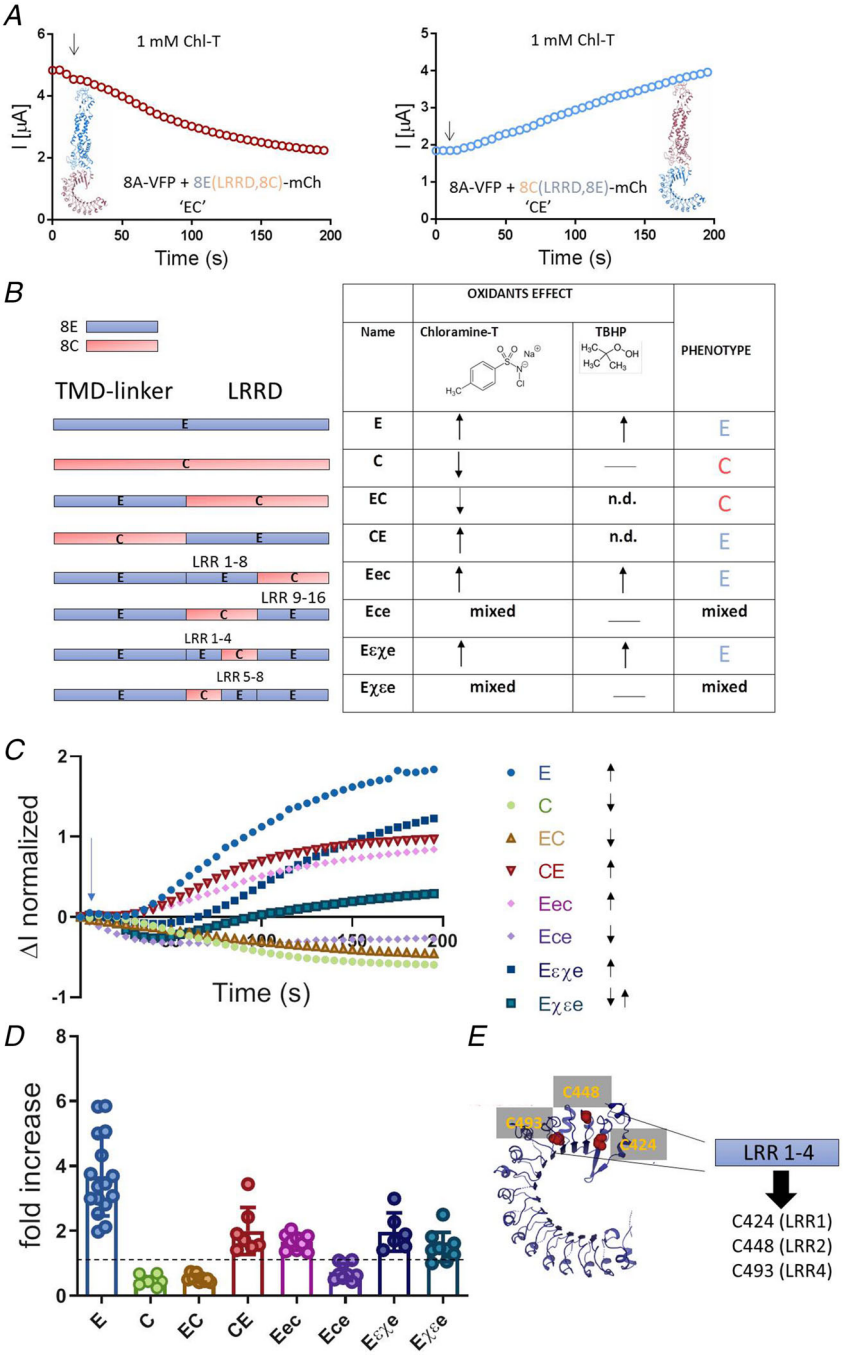

Figure 1. Chimeric strategy in oocytes to narrow down the essential target of oxidation
A, two representative traces illustrating the effect of the swap of LRR domains between 8E and 8C. Insets highlight regions that were swapped between 8E and 8C subunits to give rise to 8E(LRRD,8C) and 8C(LRRD,8E) chimeras. In red, sequences from 8C; in blue, sequences from 8E. Similar results were obtained in a total of six oocytes for 8C(LRRD,8E) and seven oocytes for 8E(LRRD,8C). Vertical arrows indicate time of Chl-T application. *B*, schematic view of all chimeras generated following the logic of the bisection method. Chimeras are denoted as CE, EC (whole LRRD swapped), Eec, Ece (half of LRRDs swapped), and Eεχe, Eχεe (first quarter of LLRDs swapped), respectively. In the table the corresponding phenotypes observed upon application of Chl-T or TBHP (colour-coded as in *A*) are highlighted. $n \geq 3$ oocytes for each chimera in each condition. Abbreviations, definition and symbol coding: 'mixed' is used to refer to a non-linear current trend (e.g. biphasic response upon oxidant application); n.d., not determined; –, no effect. Below the corresponding positions of each LRR domain in the secondary structure are listed: 8C: LRR 1–4 (426–518), LRR 5–12 (519–615), LRR 9–12 (616–711), LRR 13–16 (612–803). 8E: LRR 1–4 (419–511), LRR 5–12 (512–608), LRR 9–12 (609–704), LRR 13–16 (605–796). *C*, representative traces showing the current trend behaviour for WT channels and chimeras upon 1 mM Chl-T application. *D*, mean fold increase for WT channels and chimeras upon 1 mM Chl-T application. The dashed line at 1 point fold increase was inserted to ease the interpretation between activatory *versus* inhibitory phenotype. Unpaired *t*-test with Welch's correction was employed. Following chimeras were compared to 8A/8E ($n = 16$): EC ($n = 9$, $P < 0.0001$), Ece ($n = 9$, $P < 0.0001$), and Eχεe ($n = 9$, $P < 0.0001$). The other chimeras were compared to 8A/8C ($n = 8$): CE ($n = 7$, $P = 0.0012$), Eec ($n = 9$, $P < 0.0001$), Eεχe ($n = 6$, $P = 0.013$). *E*, the three cysteines of 8E in LRR 1–4 are highlighted. [Colour figure can be viewed at wileyonlinelibrary.com]

C448S, C493L). The choice of the mutations was based on the identity of the amino acid at the equivalent position in 8C. In full agreement with the chimeric approach, oocytes co-injected with 8A/8E(C424F–C448S–C493L) expressed currents insensitive to both Chl-T and TBHP (Fig. 2*A*, *B* and G). We next tested the single mutant 8E(C493L), which, similarly to WT 8A/8E, turned out to be sensitive to both oxidants when co-injected with 8A. This allowed us to exclude C493 as a target of oxidation (Fig. 2*C*, *G* and *H*). Conversely the double mutant 8E(C424F–C448S) co-expressed with 8A was completely insensitive to Chl-T and TBHP, suggesting that one of the two residues, C424 or C448, might be the exact target (Fig. 2*D* and *G*). Surprisingly, both single mutants, 8E(C424F) as well as 8E(C448S), proved to be insensitive to oxidant application, that is no increase of the currents was observed upon oxidant application (Fig. 2*E*, *G* and *H*). This result implies that both cysteines, C424 and C448, of 8E are targets of oxidation, and both are strictly required to elicit the potentiating effect observed upon Chl-T or TBHP application.

Reversal by dithiothreitol suggests formation of a disulfide bond between C424 and C448

We took advantage of a homology model of 8A/8E heteromeric channels to obtain further insight into the structure–function relationship of the two cysteines. C424 is localized at the C-terminus of the β-strand of LRR1 while C448 lies in the linker connecting the LRR2 β-strand and the LRR2 α-helix. This results in a 3D conformation where C424 and C448 are spatially close, almost facing one another (Fig. 2*I* and *J*). According to the homology model, C424 and C448S lie at ∼7.1 Å distance. Such a structural proximity of residues, even though relying on an approximate model, suggests that Chl-T/TBHP might mediate a reaction between the cysteines, which induces formation of a disulfide bond. Even though, *a priori*, such a distance might appear too large to be compatible with the formation of a disulfide bond, two arguments suggest that this possibility cannot be excluded. Firstly, the distance estimate is based on a homology model, which is intrinsically susceptible to inaccuracies at this level of resolution. Secondly, there is evidence that Chl-T and oxidants in general can mediate the formation of a disulfide bond when they encounter proximal cysteines with highly reactive participating thiols in close proximity (Cremers & Jakob, 2013; Rehder & Borges, 2010a, 2010b). Based on this possibility, we invoke the idea that Chl-T and TBHP induce the formation of a disulfide bond between C424 and C448. The resulting bridge could act like a mechanical pinch forcing the C-terminal ends of the LRRD toward an open conformation.

To further explore this hypothesis and assess whether Chl-T-mediated oxidation can be reverted, we perfused the oocytes with the reducing agent dithiothreitol (DTT), commonly used to disrupt disulfide bonds. 8A/8E heteromers were first activated with 1 mM Chl-T until steady state was reached, and then perfused with 10 mM DTT. As shown in Fig. 2*K*, application of DTT led to a steep decrease of the current suggesting a disruption of the structural rearrangement induced by Chl-T.

Intracellular application of a short-arm cysteine crosslinker leads to 8A/8E channel activation

To strengthen our hypothesis concerning disulfide bond formation between C424 and C448, we made use of the short-arm (8 Å) maleimide crosslinker (BMOE) suitable to establish covalent and irreversible conjugation of pairs of sulfhydryl groups (Fig. 3*A*). Crosslinking occurs only between residues with a distance of 8 Å or lower. Oocytes are not ideal for this type of experiment because it is intrinsically difficult to apply cysteine-modifying reagents via microinjection at a known effective concentration, given the large quantity of yolk that will neutralize most of the reagent. We thus tested the effect of intracellular application via the patch pipette of BMOE in LRRC8(−/−)HEK cells transfected with 8A/8E WT or with a mutant lacking the C-terminal cysteines C424 and C448 (8A/8E(C424F–C448S)) (Fig. 3).

We first performed the experiments using the untagged versions of LRRC8 subunits to exclude any interference due to the residual activity of heteromers arising from C-terminally tagged subunits (Fig. 3*A*–*C*). To identify positively transfected cells, we co-transfected a plasmid encoding the CD8 receptor protein and patched cells covered by anti-CD8 coated beads (Jurman et al., 1994). Notably, 40 μM BMOE induced a strong current activation upon whole cell access only for cells transfected with 8A/8E WT, while no effect was observed in any of the cells transfected with the 8A/8E(C424F–C448S) mutant (Fig. 3*A*–*C*). This finding clearly implies that a crosslink between C424 and C448 induces channel activation. Despite the clear trend observed upon BMOE application, the experiment is affected by the use of untagged constructs, which implies the possibility of recording non-transfected cells, that is cells expressing CD8 but little 8A/8E WT or 8A/8E(C424F–C448S).

We thus performed another set of experiments employing fluorescently tagged constructs and extended the analysis to the single mutant 8A-cer/8E(C448S) to further validate the hypothesis of a crosslink formation between the two cysteines (Fig. 3*D*–*I*). We first conducted a control experiment with standard intracellular solution lacking BMOE to exclude any tendency of the tagged heteromers to undergo spontaneous activation

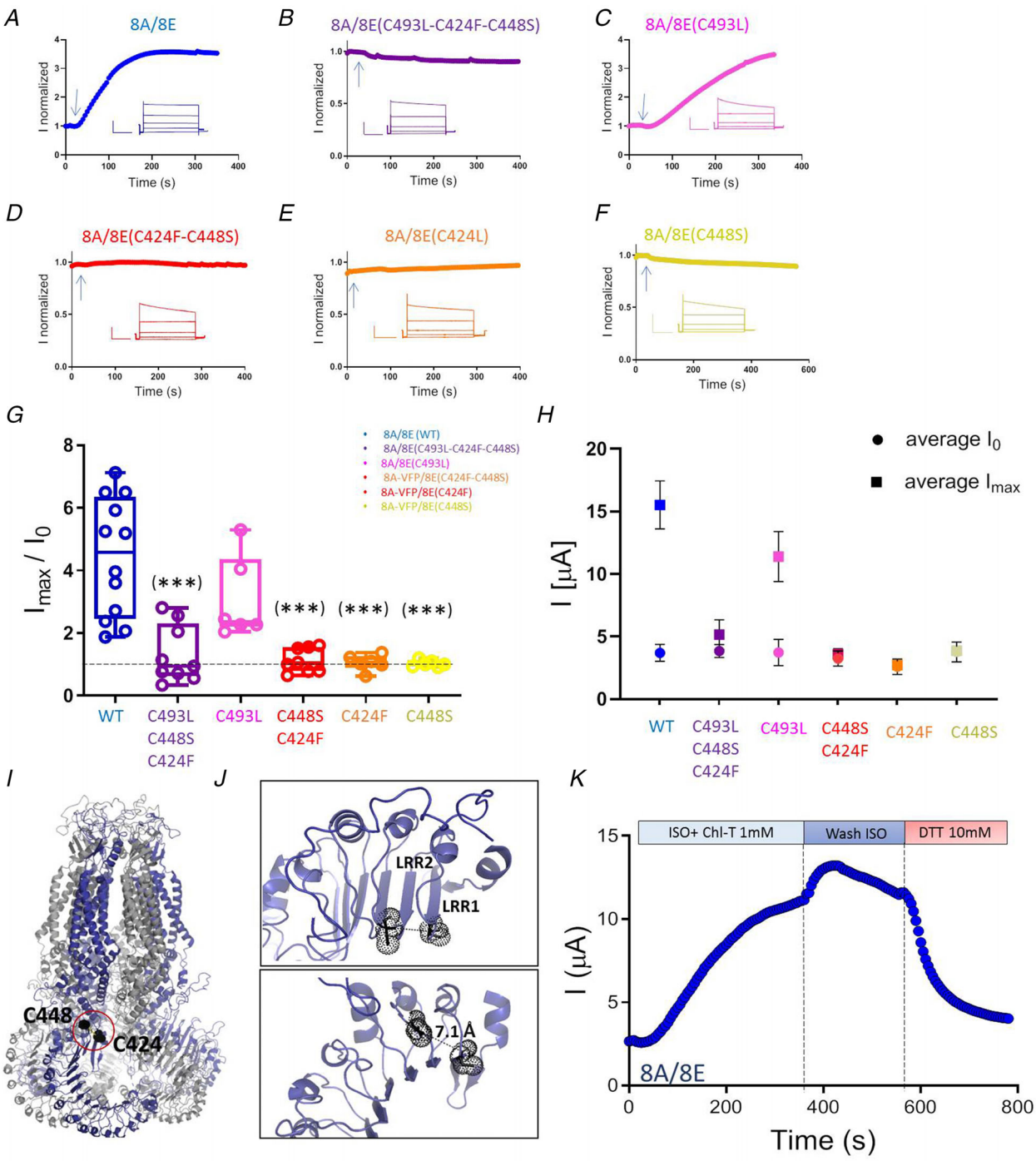

Figure 2. Effect of Chl-T in oocytes expressing 8A-VFP/8E-mCh channels harbouring different mutations in 8E

A–F, time course of currents modulation upon Chl-T application. Insets show response to an *I–V* stimulation protocol from −60 to +60 mV in steps of 40 mV before stimulus application. Scale bars (2 μA, 200 ms). Vertical arrows indicate time of Chl-T application. Oocytes were injected with 8A/8E (n = 12) (*A*), 8A/8E(C493L–C424F–C448S) (n = 9) (*B*), 8A/8E(C493L) (n = 6) (*C*), 8A/8E(C424F–C448S) (n = 8) (*D*), 8A/8E(C424L) (n = 6) (*E*), and 8A/8E(C448S) (n = 6) (*F*). *G*, box and whisker plot showing minimal and maximal fold increase for each construct. The line inside the boxes indicates the median value. The difference is statistically significant ($P < 0.0001$, one-way ANOVA). Following pairs are significantly different (Tukey–Kramer test) *versus* WT: 8A/8E(C493L–C424F–C448S), $P < 0.0001$; 8A/8E(C424F–C448S), $P < 0.0001$; 8A/8E(C424L), $P < 0.0001$; and 8A/8E(C448S); $P < 0.0001$. The difference between other groups is not significant (8A/8E(C493L): $P = 0.1359$). *H*, mean initial and final current after 5 min exposure to 1 mM Chl-T. *I*, full structural view of the hexamer

with C424 and C448 represented in one subunit as black spheres. *J*, close-up view (top and side) of C424 and C448 mutual position in the backbone of the leucine-rich repeat domain. Cysteines 424 and 448 are highlighted with dots and sticks. The distance within residues is 7.1 Å according to the model. Panels *I* and *J* were made with Pymol using the homology model of 8A/8E (8A-subunit, grey cartoon; 8E-subunit, blue cartoon). *K*, representative trace of oocytes injected with 8A/8E heteromers to show DTT reversal of Chl-T-induced current (87.1%). Similar experiments were repeated for $n = 4$ oocytes (mean reversal = 74.7 ± 24 %, SD). [Colour figure can be viewed at wileyonlinelibrary.com]

(Fig. 3*D*). Next, experiments with BMOE in the pipette solution revealed that 8A-cer/8E WT transfected cells exhibited a strong current increase, compared to both the double (8A-cer/8E(C424F–C448S)) and the single (8A-cer/8E(C448S)) mutant, for which no effect of the crosslinker was detected (Fig. 3*E*–*G* and *I*). To test for the effect of BMOE in a more physiological context, we also applied the crosslinker on non-transfected HEK cells (Fig. 3*H*). It is necessary to highlight that in the absence of a profound knowledge of the relative levels of expression of all LRRC8 subunits in these cells, the final outcome of this experiment is difficult to predict. Interestingly however, we observed an mean current increase of 3.2-fold for non-transfected HEK cells upon 40 μM BMOE (Fig. 3*I*), even though the absolute current levels were smaller compared to those elicited by BMOE in LRRC8(−/−)HEK cells transiently transfected with 8A-cer/8E. This result suggests a significant expression of the 8E subunit in HEK cells, and, most importantly, it reinforces the hypothesis of a disulfide bond formation between cysteines 424 and 448 of 8E, supporting a physiological relevance of our findings.

Transplantation of oxidation sensitivity from 8E to 8C

Interestingly, C424 and C448 are not conserved among the LRRC8 isoforms, being unique to 8E. At this stage we attempted to transplant the activation mechanism present in 8E into 8C subunits by inserting the two cysteines at the corresponding positions in LRR1 of 8C, that is I431 and K455, obtaining the 8C(I431C–K455C) construct. As mentioned above, it is important to note that differently from Chl-T that strongly inhibits 8C-containing heteromers, TBHP does not exert any effect on them, as previously published (Gradogna, Gavazzo et al., 2017). On the contrary both TBHP and Chl-T activate 8E-formed heteromers. This leaves open two possible scenarios. First, oxidation by TBHP might be of a different chemical nature. More likely, however, TBHP primarily oxidizes cysteines whereas Chl-T oxidizes also other residues. Taking advantage of this difference, we first employed TBHP to allow an easier identification of any effect introduced by the inserted cysteines. We first quantified the initial basal current for all the constructs tested in this set of experiments (Fig. 4*A*). Unlike what observed for 8A/8C, application of TBHP in oocytes expressing 8A/8C(I431C–K455C) resulted in a current increase very similar to that observed in oocytes expressing 8A/8E (Fig. 4*B*–*D* and *G*), showing that we had successfully conferred the typical 8E potentiation to 8C. We next tested Chl-T on the same construct. *A priori*, it was difficult to establish which of the two expected effects would have prevailed: activation induced by oxidation of the two introduced cysteines or inhibition mediated by the 8C background. Actually, application of Chl-T to oocytes expressing 8A-VFP/8C(I431C–K455C) led to an initial slight increase of the current (first 30 s) followed by a slow gradual decrease, which became evident only after a prolonged time (Fig. 4*E* and *F*), and with clearly different kinetics compared to the response of WT 8A/8C. Apparently, the presence of the two cysteines in the 8C background leads to a temporary initial approximate balance of the two effects, such that neither activation nor inactivation prevails (Fig. 4*E* and *F*). Only after several minutes does the inhibitory effect turn out to be predominant, leading to a slow irreversible inactivation of the current. Figure 4*E* shows two representative traces revealing that 8A/8C-mediated current is reduced to about 50% of the initial value after 3 min exposure to Chl-T while 8A/8C(I431C–K455C)-mediated currents are still close to the initial value and reach 50% only after 10 min exposure. This consistent difference in the time course of inactivation is likely explained by Chl-T reaction with the two introduced cysteines that, at the outset, compensates for the still present inhibitory effect. Indeed, this result shows that Chl-T still reacts with another, so far unknown, motif(s) present in 8C leading to a final, delayed inactivation of the channel.

Exclusion of almost all cysteines and methionines of 8C as the target of oxidation

Having unambiguously identified the two cysteine residues (C424 and C448) underlying potentiation of 8A/8E heteromers, we sought to similarly identify residues responsible of Chl-T-mediated 8A/8C inhibition. The results obtained with the first chimeras, where the LRRD between 8E and 8C were swapped, suggested that residues within the LRRD might underlie also 8C oxidation sensitivity (Fig. 1*A*). However, results obtained with the subsequent sub-chimeras were difficult to interpret (Fig. 1*B*) because of mixed effects of Chl-T. Thus, we initially considered the first half of the LRRD and mutated all cysteine and methionine residues of 8C within

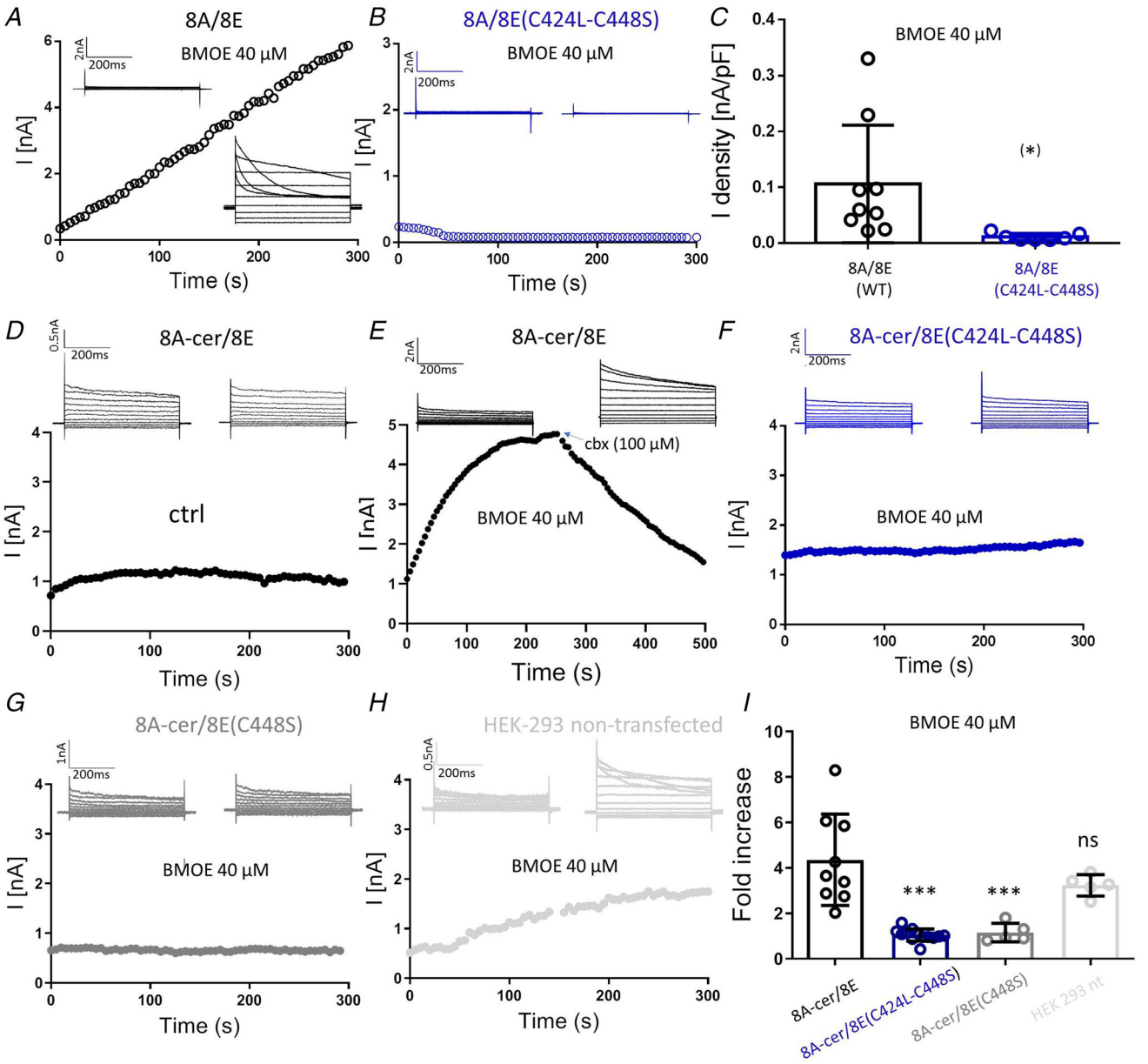

Figure 3. Effect of BMOE in transfected LRRC8(−/−)HEK cells and non-transfected WT HEK cells
Experiments in *A*–*G* were performed in LRRC8(−/−)HEK cells. *A* and *B*, representative traces showing the time course of non-tagged 8A/8E WT and 8A/8E(C424L–C448S)-mediated current upon intracellular application of 40 μM BMOE. The upper left panel shows the *I*–*V* response upon whole cell access, while in the bottom panel (or upper right *B*) is the *I*–*V* response 5 min after BMOE application. *C*, mean current density of cells transfected with 8A/8E WT (n = 9) or 8A/8E(C424L–C448S) (n = 7) 5 min after BMOE stimulation. The difference is statistically significant (P = 0.0267, unpaired t-test with Welch's correction). *D*–*H*, representative traces showing the time course of current mediated by transiently transfected tagged constructs. *D* displays 8A-cer/8E current change upon intracellular standard solution while *E*–*H* display current change upon intracellular application of 40 μM BMOE for 8A-cer/8E (*E*), 8A-cer/8E(C424L–C448S) (*F*), 8A-cer/8E(C448S) (*G*), and non-transfected HEK (*H*). The upper left insets show the *I*–*V* response upon whole cell access, while the upper right insets display the *I*–*V* response 5 min after BMOE application. Average basal and final current densities were determined: 8A-cer/8E (n = 9), 51.6 ± 32.8 to 234.6 ± 40.1 pA/pF; 8A-cer/8E(C424L–C448S) (n = 13), 26.67 ± 15.62 to 28.9 ± 17.19 pA/pF; 8A-cer/8E(C448S) (n = 5), 38.1 ± 20.1 to 40.3 ± 22.4 pA/pF; HEK nt (n = 5), 9.8 ± 6.4 to 29.1 ± 17.2 pA/pF. *I*, fold increase of current change of respectively, WT, mutants and non-transfected HEK cells, respectively, after 5 min exposure to intracellular BMOE. In *I* unpaired t-test with Mann–Whitney's correction (*vs.* 8A-cer/8E n = 9): 8A-cer/8E(C424L–C448S) (n = 13, $P < 0.0001$); 8A-cer/8E(C448S) (n = 5, P = 0.001), HEK nt (n = 5, P = 0.4376, ns). [Colour figure can be viewed at wileyonlinelibrary.com]

this region (LRR 1−8). However, none of the mutants abolished the Chl-T inhibitory effect (Table 1). We thus extended mutagenesis to all cysteine and methionine residues within the entire LRRD domain, but again this approach failed to identify a good candidate (Table 1). We therefore concluded that for the specific case of the 8C subunit, the chimeric strategy was misleading (as discussed in depth in the Discussion).

We proceeded to screen all methionines and most cysteines (excluding those involved in cysteine bridges in the extracellular domains) of the full length 8C subunit. Since there is evidence that hypochlorite can also oxidize histidine residues, even though at a lower rate (Hawkins et al., 2003), we selected several histidines in the LRRD. Again, none of the candidate mutations turned out to abolish or attenuate Chl-T-mediated inhibition (Table 1).

Identification of the first methionine of 8C as the target of oxidation using concatemers with a self-cleavable peptide

The only residue we excluded from the above screening was the start methionine of 8C (M1), in that M1 is essential for initializing protein synthesis. Furthermore, the N-terminus of LRRC8 proteins has been shown to be essential for channel functioning with several mutants within the first 15 amino acids resulting in a loss of function of VRACs (Zhou et al., 2018). Since the first methionine is mandatory for the initiation of protein synthesis, it is intrinsically difficult to modify, and we needed to find a strategy to bypass this constraint. A simple approach might be to use a concatemer of 8A and 8C subunits in which the 8C start methionine could be mutated at will. However, it has been shown that the N-terminus of LRRC8 subunits must be 'free' to form functional channels (T. J. Jentsch, personal communication). To circumvent this problem, we employed a self-cleaving peptide sequence (T2A) able to physically separate 8A and 8C subunits in the concatemer (Tang et al., 2009) (see Methods). While this is encoded by only one mRNA, the cleavage at the translational level produces two distinct peptides. We generated two variants: a control concatemer 8A–8C(M) supposed to mimic WT 8A/8C heteromeric channels, and a concatemer in which M1 of 8C was replaced with a leucine residue, 8A–8C(L).

Concatemers expressed in *Xenopus* oocytes yielded currents significantly above background but much lower

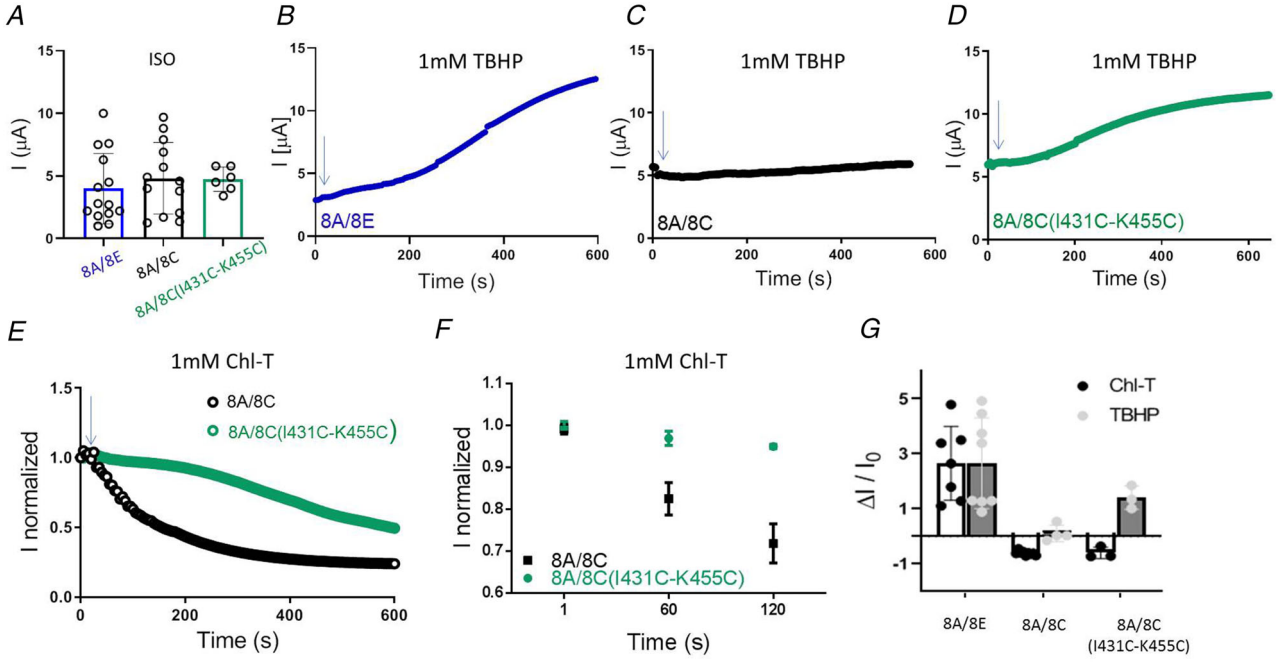

Figure 4. Characterization of 8A/8C(I431C–K455C) mutant in oocytes
A, quantification of recorded basal current (individual as well as mean value) for each different channel. *B–D*, representative traces of 8A/8E (*B*), 8A/8C (*C*) and 8A/8C(I431C–K455C) (*D*) current upon application of *tert*-butyl hydroperoxide (TBHP). *E*, Normalized current traces of 8A/8C(I431C–K455C) and 8A/8C highlighting differences in the time course of inactivation after Chl-T application. *F*, plot of mean ± SD amplitudes at 1, 60 and 120 s after Chl-T application. *G*, bar charts showing mean fold current change after 5 min exposure to Chl-T and TBHP to oocytes expressing 8A/8E (n = 7, Chl-T; n = 8, TBHP), 8A-VFP/8CmCh (n = 9, Chl-T; n = 4, TBHP) and 8A/8C(I431C–K455C) (n = 3, P = 0.934, Chl-T; n = 3, P = 0.015, TBHP). [Colour figure can be viewed at wileyonlinelibrary.com]

Table 1. List of single-point mutations of 8C-mCh without effect

	Domain
8C-Met residues mutated	
M48L	ECL1
M96L	ECL1
M114L	ECL1
M139L	TM2
M193L	TM2-TM3 linker
M300L	ECL2
M312L	ECL2
M376L	TM4-LRR linker
M432L	LRRD
M458T	LRRD
M503L	LRRD
M510L	LRRD
M570L	LRRD
M581L	LRRD
M588L	LRRD
M800L	LRRD
8C-Cys residues mutated	
C477S	LRRD
C493F	LRRD
C571S	LRRD
C599S	LRRD
C682S	LRRD
C715S	LRRD
C728S	LRRD
C774S	LRRD
8C-His residues mutated	
H423N	LRRD
H475N	LRRD
H482N	LRRD
H527N	LRRD
H598N	LRRD
H669N	LRRD
H678N	LRRD
H763N	LRRD
H423N	LRRD
H475N	LRRD

than those obtained by co-expressing the single subunits (see caption of Fig. 5*A*). Nevertheless, the application of a hypotonic solution elicited a swelling-dependent current response comparable among different mutants, reproducing the typical behaviour of VRAC currents (Fig. 5*A*). We then assessed the effect of oxidation. The control concatemer 8A–8C(M) was consistently inhibited by Chl-T (Fig. 5*B* and *C*). Most importantly, currents measured in oocytes injected with 8A–8C(L), in which the start methionine of 8C is mutated to leucine, were insensitive to Chl-T (Fig. 5*B* and *C*).

These results strongly suggest that oxidation of the start methionine of 8C subunits underlies inhibition of 8A/8C heteromers. To further cement this conclusion, we inserted into the 8A–8C(L) concatemer the two cysteine residues at positions 431 and 455 that conferred activation by TBHP to 8C subunits (construct 8A–8C(LCC)). Indeed, the application of TBHP to the 8A–8C(LCC) concatemer resulted in a significant increase of currents (data not shown), confirming that the concatemer is able to reproduce the results obtained by co-injection of the single subunits. More importantly, also the application of Chl-T led to a strong activation of currents (Fig. 5*B* and *C*), demonstrating the absence of the inhibitory effect of Chl-T seen in WT 8A/8C heteromers. Furthermore, DTT application rapidly reverted the Chl-T-induced activation (Fig. 5*D*), in a manner compatible with disulfide disruption, again reproducing the 8E phenotype.

Interestingly, 8A–8C(MCC) (i.e. channels with intact 8C start methionine and introduced activating cysteines from 8E) displayed a moderate current activation upon Chl-T perfusion (Fig. 5*B* and *C*). This might seem at odds with the overall inhibitory effect of Chl-T on currents induced by the 'equivalent' injection of 8A/8C(I431C–K455C) (Fig. 4*C* and *D*). This apparent discrepancy might be related to the fact that concatemers generated with the T2A linker introduce small changes both at the C-terminal end of the first peptide and at the N-terminal end of the second peptide. In particular, a proline residue is left over in front of the second peptide. Thus, in the construct 8A–8C(MCC) M1 of 8C is preceded by a proline residue which might partially diminish the effect of oxidation on channel activation. In contrast, the inserted cysteines (I431C–K455C) are not affected by the concatemeric strategy, which might explain prevalence of the activatory response. Moreover, the addition of a proline residue might explain the overall smaller expression levels elicited by expression of concatemers. This is also coherent with previous findings concerning the relevance of the N-terminus for VRAC functioning (Zhou et al., 2018).

Confirmation of oxidation targets in LRRC8(−/−)HEK cells

To further corroborate our data in a complementary heterologous expression system and assess the general validity of our findings, we employed the LRRC8(−/−)HEK cell line. First of all, we performed a detailed analysis of WT channel response to Chl-T by employing both non-tagged and C-terminally tagged constructs (8A/8E and 8A/8C or 8A-cer/8E and 8A-cer/8C). All tested combinations nicely recapitulated the phenotype observed in oocytes: 8E- and 8C-formed heteromers were respectively enhanced and inhibited when perfused with 1 mM Chl-T, regardless of the presence or not of the fluorescent tag at the

C-terminus (Fig. 6*A*–*B*, *G* and *H*). Notably, the set of experiments carried out with non-tagged constructs further corroborate the idea that oxidation of 8A/8E channels is a sufficient stimulus to fully activate initially inactive channels (Fig. 6*A*). We then assessed the effect of Chl-T on the mutant channels 8A-cer/8E(C424L–C448S) and 8A-cer/8E(C448S). The measurements of the single and the double mutant for the two proximal cysteines confirmed the abolishment of Chl-T effect in the 8E background (Fig. 6*E*–*G*).

Once the trend of current modulation upon Chl-T application was established for channels generated by the co-expression of separate subunits, the following step was to test the concatemeric strategy in LRRC8(−/−)HEK cells. To this end we sub-cloned 8A–8C(M), 8A–8C(L) and 8A–8C(LCC) concatemers in a mammalian expression vector (König et al., 2019). Transfection of LRRC8(−/−)HEK with these concatemers resulted in fluorescence at the level of the plasma membrane (Fig. 7*A*), confirming correct trafficking of both subunits. All concatemers exhibited a variable and relatively large constitutive current upon whole cell access (Fig. 7*B*), as expected by the presence of a tag at the C-terminus of each subunit (Gaitán-Peñas et al., 2016; König et al., 2019). Currents elicited by 8A–8C(M), 8A–8C(L) and 8A–8C(LCC) were indistinguishable and displayed typical slow inactivation of WT 8A/8C currents (Fig. 7*C*). This allowed us to rule out a possible effect of the M1L mutation on the kinetics of inactivation. All concatemers gave rise to channels capable of undergoing further activation upon hypotonic stimulation, resulting in a similar fold increase (Fig. 7*C* and *D*).

We next explored the effect of oxidation. The application of Chl-T on cells transfected with the 8A–8C(M) control concatemer resulted in a marked inhibition of the constitutive current (Fig. 7*E*–*G*). In contrast, application of 1 mM Chl-T to cells expressing the 8A–8C(L) concatemer resulted in variable effects on current amplitudes that sometimes included a slight initial current increase followed by a decrease below the level of the initial constitutive current, resulting in practically no change of current amplitude (Fig. 7*E*–*G*). Notably, Chl-T elicited a strong potentiation of LCC-mediated currents (Fig. 7*E*–*G*), similarly to what observed in oocytes, which was sometimes followed by a variably pronounced decrease resulting in an overall ∼2-fold increase (Fig. 7*E* and *G*).

The results confirm that the first methionine of 8C is mostly responsible for Chl-T-mediated current inhibition also in LRRC8(−/−)HEK cells.

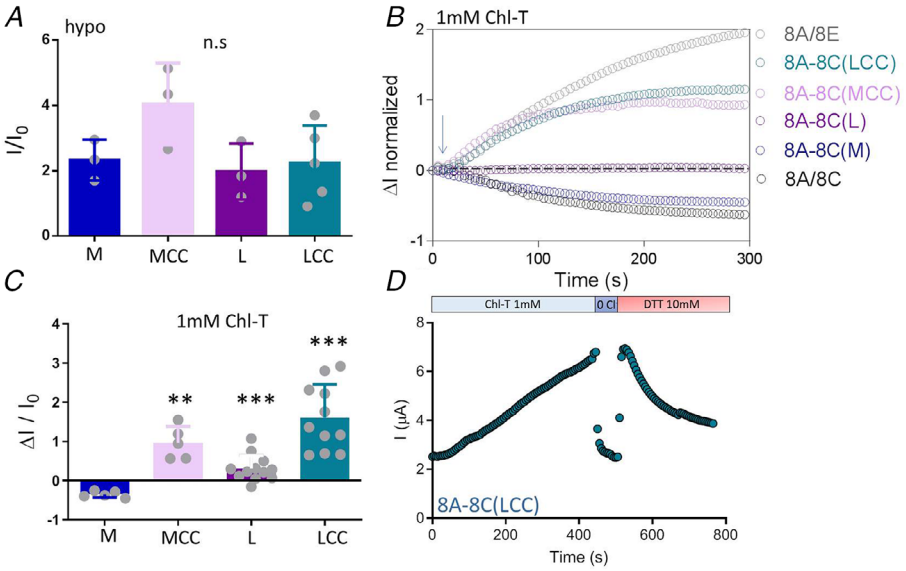

Figure 5. The first methionine of 8C subunit is the target of chloramine-T
All experiments presented in this figure were performed in oocytes. The mean initial current (I_0) was: 8A–8C(M), 1.53 μA; 8A–8C(MCC), 1.18 μA; 8A–8C(L), 1.29 μA; and 8A–8C(LCC), 1.21 μA, respectively. *A*, currents recorded 5 min after hypotonic stimulation are normalized to the initial constitutive current. *B*, Representative traces of 8A/8E, 8A–8C(LCC), 8A–8C(L), 8A/8C and 8A–8C(M) illustrate that the first methionine (M1) of 8C is the target of Chl-T. *C*, normalized current change ($\Delta I/I$ initial) upon application of 1 mM Chl-T. The same protocol of 200 ms pulses every 5 s at 60 mV was applied both in *A* and *C*. *D*, representative trace showing the effect of DTT (10 mM) after Chl-T in an oocyte injected with 8A–8C(LCC) ($n = 3$). In *C* unpaired *t*-test with Welch's correction (*vs*. 8A–8C(M) $n = 5$): 8A–8C(MCC) ($n = 5$, $P = 0.0019$); 8A–8C(L) ($n = 12$, $P < 0.0001$); and 8A–8C(LCC) ($n = 11$, $P < 0.0001$). [Colour figure can be viewed at wileyonlinelibrary.com]

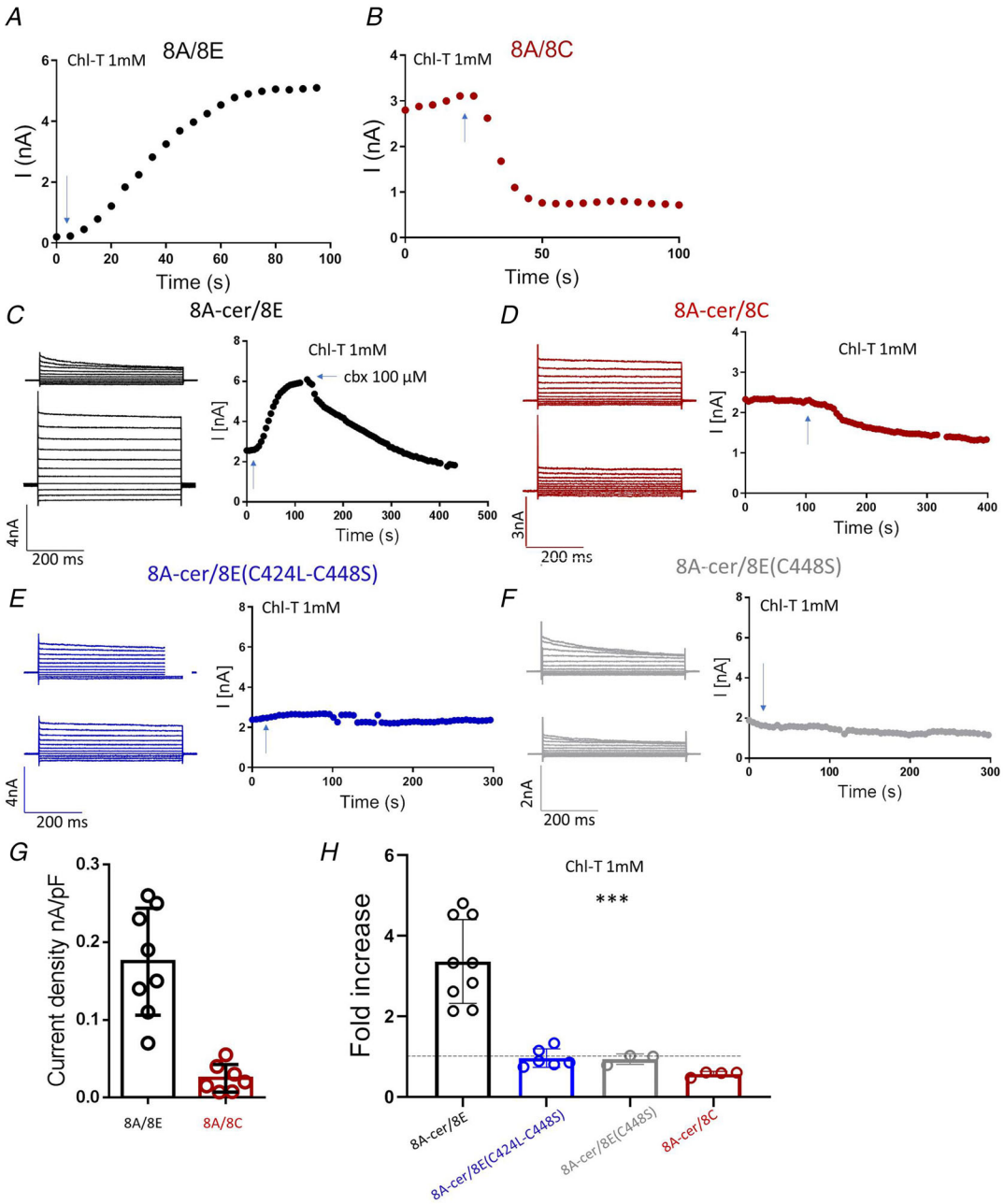

Figure 6. Characterization of Chl-T effect on transiently transfected LRRC8(−/−)HEK cells
A and *B*, representative time course currents mediated by 8A/8E and 8A/8C upon Chl-T application to show the modulation of channels generated by the transfection of non-tagged constructs. Similar experiments were performed for $n = 8$ (8A/8E) and $n = 7$ (8A/8C). *C–F*, representative *I–V* responses upon whole cell access (upper panel) and after 5 min exposure to Chl-T (bottom panel) for 8A-cer/8E, 8A-cer/8C, 8A-cer/8E(C424L–C448S) and 8A-cer/8E(C448S), respectively. Vertical arrows indicate time of Chl-T application. Similarly, on the right are displayed representative traces showing the time course of current modulation upon Chl-T application (1 mM). For the experiment with 8A-cer/8E (*C*), 100 μM CBX was applied to verify that currents are mediated by VRACs. Note that only the 8A subunit is tagged with the cerulean fluorescent protein in these experiments. *G*, current density of non-tagged channels 8A/8E ($n = 8$) and 8A/8C ($n = 7$) after 5 min exposure to 1 mM Chl-T. Unpaired *t*-test with Welch's correction, $P < 0.001$. *H*, mean current fold increase after 5 min exposure to Chl-T for both WT and mutant tagged channels. Mean basal and final current were determined: 8A-cer/8E, 2.6 ± 1.1 to 8.1 ± 2.4 nA; 8A-cer/8E(C424L–C448S), 2.8 ± 1.4 to 2.78 ± 1.5 nA; 8A-cer/8E(C448S) 2.5 ± 1.3 to 2.78 ± 1.4 nA; and 8A-cer/8C, 2.3 ± 1.2 to 1.28 ± 0.9 nA. Unpaired *t*-test with Welch's correction (*vs*. 8A-cer/8E, $n = 9$): 8A-cer/8E(C424L–C448S) ($n = 5$, $P < 0.0001$); 8A-cer/8E(C448S) ($n = 3$, $P < 0.0001$); and 8A/8C ($n = 4$, $P < 0.0001$). [Colour figure can be viewed at wileyonlinelibrary.com]

Discussion

The functional coupling between VRAC activity and ROS is very little understood. Given the broad physiological and pathophysiological relevance of VRAC sensitivity to ROS it is important to decipher the molecular mechanisms underlying this regulation. An important matter of debate is whether ROS directly act on VRACs or indirectly through the modulation of upstream regulators. A previous report provided evidence that Chl-T and TBHP have divergent effects when applied on oocytes injected with 8A/8E compared to those injected with 8A/8C or 8A/8D subunits, and suggested a direct oxidation of intracellular cysteines of 8E and of methionines of 8C (Gradogna, Gavazzo et al., 2017). However, which residues were affected by oxidation remained unclear. In addition, it was not fully resolved earlier if oxidation of 8A/8E heteromers can activate these channels '*de novo*', or only augments channels preactivated, for example by fluorescent tags.

In the present work we identified the targets of oxidation in 8E as well as in 8C subunits. Based on successive chimeras of 8E and 8C subunits, we revealed C424 and C448 of 8E as the targets of Chl-T and TBHP oxidation. Both cysteines are essential to elicit the strong potentiation of VRAC activity upon oxidant application: if one of them is mutated, the responsiveness to Chl-T and TBHP is abolished. Results with untagged constructs additionally showed that pre-stimulation is not necessary for oxidation or crosslinker-mediated 8A/8E activation, but that the channels can be fully activated

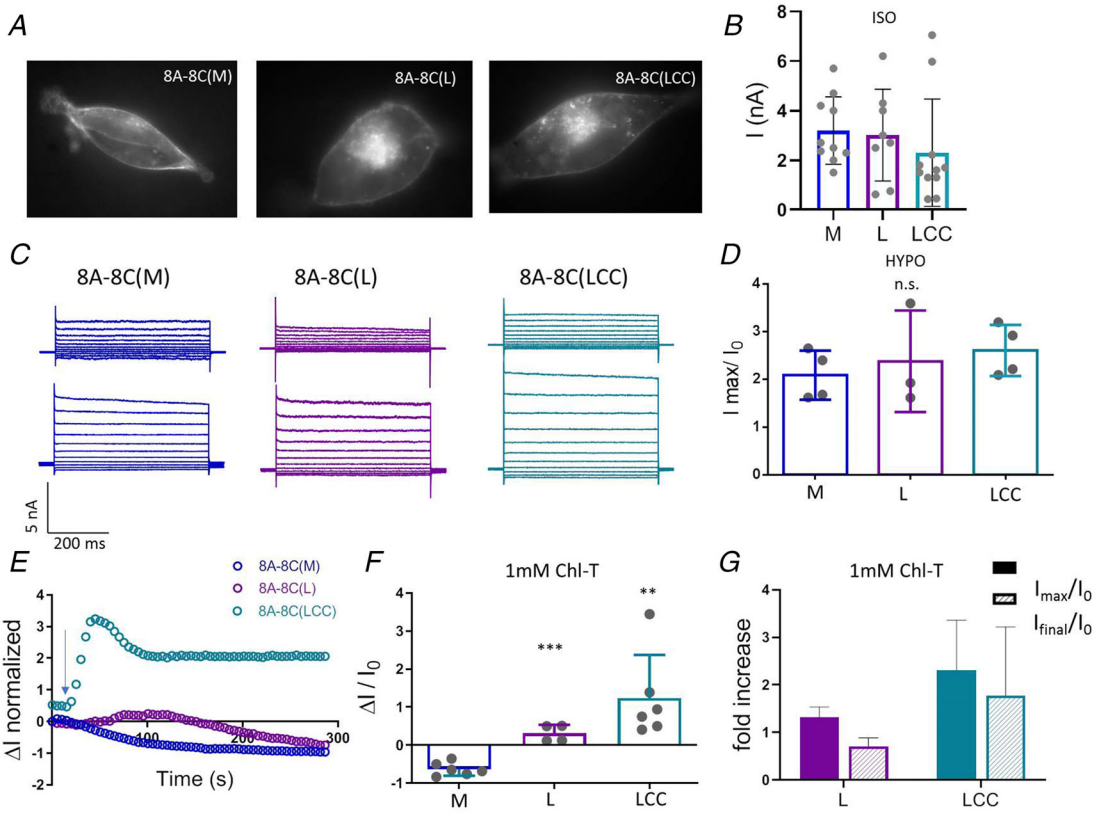

Figure 7. Effect of concatemers expression and Chl-T application in LRRC8(−/−)HEK cells
A, fluorescence is visible at the plasma membrane level confirming the correct trafficking of the channel and the success of the concatemeric strategy. For each cell, images were acquired at excitation wavelengths of λ = 480/560 nm (VFP and mCherry, respectively). *B*, mean basal current of 8A–8C(M), $n = 10$, 8A–8C(L), $n = 8$, and 8A–8C(LCC), $n = 11$. *C*, representative *I–V* traces of 8A–8C(M), 8A–8C(L), and 8A–8C(LCC) concatemers before (upper panel) and after (lower panel) hypotonic stimulation. All constructs display the typical slow inactivation of WT 8A/8C. *D*, mean fold increase of current mediated by different concatemers upon hypotonic stimulation (I_{max}/I_0); (8A–8C(M), $n = 4$, 8A–8C(L), $n = 3$, and 8A–8C(LCC), $n = 4$). *E*, representative time course current recordings of 8A–8C(M), 8A–8C(L) and 8A–8C(LCC) upon 1 mM Chl-T application (5 min). *F*, mean fold change of current after 2 min perfusion with 1 mM Chl-T ($\Delta I/I_0$). Note that ΔI is ($I_{max} - I_0$) for 8A–8C(L) and 8A–8C(LCC), and ($I_{min} - I_0$) for 8A–8C(M). Unpaired *t*-test with Welch's correction *versus* 8A–8C(M) ($n = 6$) was employed: 8A–8C(L) ($n = 4$, $P = 0.0006$) and 8A–8C(LCC) ($n = 6$, $P = 0.0096$). *G*, mean fold increase showing I_{max}/I_0 (left) and I_{final}/I_0 (right) to highlight the effect of Chl-T application. For 8A–8C(L) and 8A–8C(LCC) concatemers, I_{max} indicates the maximal current amplitude observed for each recording, while I_{final} is the current recorded after 5 min perfusion with Chl-T. [Colour figure can be viewed at wileyonlinelibrary.com]

'*de novo*' by these stimuli. Interestingly, the two cysteines are close to each other in the 3D structure, with C424 localized at the beginning of LRR1 and C448 at the beginning of LRR2. We propose that Chl-T/TBHP induces formation of a disulfide bond between the two cysteines. In the homology model of 8A/8E heteromers, the distance between the two cysteines is around 7 Å. Such a distance might not be compatible with a direct formation of a disulfide bond that usually occurs when two cysteines are spatially closer (within 3 Å). However, it must be considered that the distance is based on a homology model built on the homomeric and unphysiological hexameric 8A structure. Being a model, it is difficult to predict the exact spatial distance of the two cysteine residues in the native conformation. However, there is considerable evidence regarding the potential role of oxidants in mediating disulfide bond formation. When reactive cysteine thiols meet reactive oxygen, sulfenic acid (RSOH) formation occurs. Sulfenic acids are highly unstable oxidation intermediates that rapidly interact with nearby cysteines to form inter- or intra-molecular disulfide bonds (RSSR), making this a primary route for oxidant-mediated disulfide bond formation (Cremers & Jakob, 2013). The formation of an intramolecular disulfide bond can bring closer two cysteines that are distant in the reduced form leading to conformational changes that might affect the function of proteins. Notably, the results obtained employing the BMOE crosslinker in LRRC8(−/−)HEK cells strongly supported the hypothesis that formation of a disulfide bond between C424 and C448 underlies oxidation-mediated activation in that BMOE induces a dramatic activation of 8A/8E WT channels, whereas no effect is observed for the 8A/8E(C424F–C448S) mutant. This finding leads to two major conclusions: first, the distance between C424 and C448 predicted by the homology model seems to be reliable, supporting the assumption that Chl-T/TBHP induces formation of a disulfide bond. Additionally, the results clearly show that a crosslink between the two cysteines leads to channel activation. The location of the two cysteines in the LRRD reinforces the relevance of C-terminal rearrangements for VRAC gating.

Interestingly, insertion of the two cysteines in the corresponding positions in the 8C subunit, which normally is not functionally modified by TBHP, resulted in TBHP-sensitive channels. This result strengthens the conclusion that a constriction within the initial LRRD leads to channel activation.

The chimeric strategy that led to the identification of the relevant oxidation targets in 8E was inconclusive in 8C. Even an exhaustive screening of all cysteines and methionines did not reveal the relevant target. The only methionine left out in the mutagenic screening was the start methionine (M1). Since the N-terminus of LRRC8 subunits has to be free (T. J. Jentsch, personal communication), we employed concatemers using the T2A cleavable-linker technology, allowing the mutation of M1, even though a proline is added in front of M1 after ribosomal cleavage. Nevertheless, the control concatemer with un-mutated M1 (8A–8C(M)) was as sensitive to Chl-T as channels obtained by co-expressing 8A and 8C. Importantly, mutating M1 to L abolished Chl-T sensitivity, revealing M1 as the target of 8C oxidation in 8A/8C heteromers. The N-terminus of LRRC8 subunits was previously reported to be critical for channel gating and some mutations altered ion selectivity (Zhou et al., 2018). Moreover, whole-cell currents mediated by 8A-T5C/8C are strongly suppressed upon the addition of extracellular (2-sulfonatoethyl)methanethiosulfonate (Kefauver et al., 2018). All these findings suggested that the N-terminus might line the cytoplasmic side of the VRAC pore folding back into the ion permeation pathway. We speculate that M1 is part of a constriction narrow enough to block the pore upon covalent modification by Chl-T. However, a critical open question is why the oxidation of the first methionine has an inhibitory effect only in 8C. Indeed, the chimera 'EC', which contains the N-terminus of 8E, is inhibited by Chl-T (Fig. 1 *A* and *B*). In retrospect, this is a highly puzzling finding. It suggests that the oxidation of M1 *per se* is not sufficient to cause channel inhibition. In fact, the results with the chimera 'EC' indicate that also the start methionine of 8E is oxidized by Chl-T, but an inhibitory effect is only observed if the LRRD is from the 8C subunit. Since oxidized methionines have one or two oxygen atoms added to the sulfur atom, the oxidized Meth side chain is bulkier. Thus, it is tempting to speculate that an N-terminus with oxidized M1 is able to occlude the pore if the LRRD is from 8C but not if it is from 8E. This scenario points again to a highly critical role of the conformation of the LRR domains for channel activation. Coincidently, this is the same conclusion we obtained regarding the disulfide bond formation in 8E subunits: bringing closer to each other C424 and C448 in LRR1 by a few angstroms leads to strong channel activation. Nicely, experiments conducted in LRRC8(−/−)HEK cells qualitatively recapitulate the results obtained in oocytes. Slight quantitative differences seen in the two expression systems might be related to the effective concentration of Chl-T, which is likely lower in oocytes because of substantial buffering by intracellular yolk.

Overall, our results provide important insights into the mechanism of channel activation and the involvement of specific molecular elements of the LRRDs and the N-terminus. The finding that a constriction introduced by the disulfide bond in LRR1-2 leads to channel activation, suggests that a similar conformational change is achieved in the general swelling induced channel gating. The possibility of disulfide bond formation in 8E subunits could be an intriguing mechanism to sense locally generated ROS in specific conditions of oxidative stress.

This question requires further investigation. In light of our findings, it would be interesting to investigate whether a variable subunit composition of VRACs in different cell types might be relevant in determining the effect of ROS, and if a specific subunit composition is required to meet physiological demands according to specific cell functions.

References

Abascal, F., & Zardoya, R. (2012). LRRC8 proteins share a common ancestor with pannexins, and may form hexameric channels involved in cell-cell communication. *Bioessays*, **34**(7), 551–560.

Bertelli, S., Remigante, A., Zuccolini, P., Barbieri, R., Ferrera, L., Picco, C., Gavazzo, P., & Pusch, M. (2021). Mechanisms of activation of LRRC8 volume regulated anion channels. *Cellular Physiology and Biochemistry*, **55**, 41–56.

Browe, D. M., & Baumgarten, C. M. (2004). Angiotensin II (AT1) receptors and NADPH oxidase regulate Cl-current elicited by beta1 integrin stretch in rabbit ventricular myocytes. *Journal of General Physiology*, **124**(3), 273–287.

Cahalan, M. D., & Lewis, R. S. (1988). Role of potassium and chloride channels in volume regulation by T lymphocytes. *Society of General Physiologists Series*, **43**, 281–301.

Cremers, C. M., & Jakob, U. (2013). Oxidant sensing by reversible disulfide bond formation. *Journal of Biological Chemistry*, **288**(37), 26489–26496.

Deneka, D., Sawicka, M., Lam, A. K. M., Paulino, C., & Dutzler, R. (2018). Structure of a volume-regulated anion channel of the LRRC8 family. *Nature*, **558**(7709), 254–259.

Ferrera, L., Barbieri, R., Picco, C., Zuccolini, P., Remigante, A., Bertelli, S., Fumagalli, M. R., Zifarelli, G., La Porta, C. A. M., Gavazzo, P., & Pusch, M. (2021). TRPM2 oxidation activates two distinct potassium channels in melanoma cells through intracellular calcium increase. *International Journal of Molecular Sciences*, **22**(16), 8359.

Friard, J., Corinus, A., Cougnon, M., Tauc, M., Pisani, D. F., Duranton, C., & Rubera, I. (2019). LRRC8/VRAC channels exhibit a noncanonical permeability to glutathione, which modulates epithelial-to-mesenchymal transition (EMT). *Cell Death & Disease*, **10**(12), 925.

Gaitán-Peñas, H., Gradogna, A., Laparra-Cuervo, L., Solsona, C., Fernández-Dueñas, V., Barrallo-Gimeno, A., Ciruela, F., Lakadamyali, M., Pusch, M., & Estévez, R. (2016). Investigation of LRRC8-mediated volume-regulated anion currents in *Xenopus* oocytes. *Biophysical Journal*, **111**(7), 1429–1443.

Gaitán-Peñas, H., Pusch, M., & Estevez, R. (2018). Expression of LRRC8/VRAC currents in Xenopus oocytes: Advantages and caveats. *International Journal of Molecular Sciences*, **19**(3), 719.

Gradogna, A., Gaitan-Penas, H., Boccaccio, A., Estevez, R., & Pusch, M. (2017). Cisplatin activates volume sensitive LRRC8 channel mediated currents in *Xenopus* oocytes. *Channels*, **11**(3), 254–260.

Gradogna, A., Gavazzo, P., Boccaccio, A., & Pusch, M. (2017). Subunit-dependent oxidative stress sensitivity of LRRC8 volume-regulated anion channels. *Journal of Physiology*, **595**(21), 6719–6733.

Hawkins, C. L., Pattison, D. I., & Davies, M. J. (2003). Hypochlorite-induced oxidation of amino acids, peptides and proteins. *Amino Acids*, **25**(3–4), 259–274.

Hazama, A., & Okada, Y. (1988). Ca^{2+} sensitivity of volume-regulatory K^+ and Cl^- channels in cultured human epithelial cells. *Journal of Physiology*, **402**(1), 687–702.

Jentsch, T. J. (2016). VRACs and other ion channels and transporters in the regulation of cell volume and beyond. *Nature Reviews. Molecular Cell Biology*, **17**(5), 293–307.

Jurman, M. E., Boland, L. M., Liu, Y., & Yellen, G. (1994). Visual identification of individual transfected cells for electrophysiology using antibody-coated beads. *Biotechniques*, **17**, 876–881.

Kasuya, G., Nakane, T., Yokoyama, T., Jia, Y., Inoue, M., Watanabe, K., Nakamura, R., Nishizawa, T., Kusakizako, T., Tsutsumi, A., Yanagisawa, H., Dohmae, N., Hattori, M., Ichijo, H., Yan, Z., Kikkawa, M., Shirouzu, M., Ishitani, R., & Nureki O. (2018). Cryo-EM structures of the human volume-regulated anion channel LRRC8. *Nature Structural & Molecular Biology*, **25**, 797–804.

Kefauver, J. M., Saotome, K., Dubin, A. E., Pallesen, J., Cottrell, C. A., Cahalan, S. M., Qiu, Z., Hong, G., Crowley, C. S., Whitwam, T., Lee, W. H., Ward, A. B., & Patapoutian, A. (2018). Structure of the human volume regulated anion channel. *eLife*, **7**, e38461.

Kern, D. M., Oh, S., Hite, R. K., & Brohawn, S. G. (2019). Cryo-EM structures of the DCPIB-inhibited volume-regulated anion channel LRRC8A in lipid nanodiscs. *eLife*, **8**, e42636.

König, B., Hao, Y., Schwartz, S., Plested, A. J., & Stauber, T. (2019). A FRET sensor of C-terminal movement reveals VRAC activation by plasma membrane DAG signaling rather than ionic strength. *eLife*, **8**, e45421.

Lee, C. C., Freinkman, E., Sabatini, D. M., & Ploegh, H. L. (2014). The protein synthesis inhibitor blasticidin s enters mammalian cells via leucine-rich repeat-containing protein 8D. *Journal of Biological Chemistry*, **289**, 17124–17131.

Lutter, D., Ullrich, F., Lueck, J. C., Kempa, S., & Jentsch, T. J. (2017). Selective transport of neurotransmitters and modulators by distinct volume-regulated LRRC8 anion channels. *Journal of Cell Science*, **130**, 1122–1133.

Nakamura, R., Numata, T., Kasuya, G., Yokoyama, T., Nishizawa, T., Kusakizako, T., Kato, T., Hagino, T., Dohmae, N., Inoue, M., Watanabe, K., Ichijo, H., Kikkawa, M., Shirouzu, M., Jentsch, T. J., Ishitani, R., Okada, Y., & Nureki, O. (2020). Cryo-EM structure of the volume-regulated anion channel LRRC8D isoform identifies features important for substrate permeation. *Communications Biology*, **3**(1), 240.

Okada, Y., Okada, T., Sato-Numata, K., Islam, M. R., Ando-Akatsuka, Y., Numata, T., Kubo, M., Shimizu, T., Kurbannazarova, R. S., Marunaka, Y., & Sabirov, R. Z. (2019). Cell volume-activated and volume-correlated anion channels in mammalian cells: Their biophysical, molecular, and pharmacological properties. *Pharmacological Reviews*, **71**(1), 49–88.

Planells-Cases, R., Lutter, D., Guyader, C., Gerhards, N. M., Ullrich, F., Elger, D. A., Kucukosmanoglu, A., Xu, G., Voss, F. K., Reincke, S. M., Stauber, T., Blomen, V. A., Vis, D. J., Wessels, L. F., Brummelkamp, T. R., Borst, P., Rottenberg, S., & Jentsch, T. J. (2015). Subunit composition of VRAC channels determines substrate specificity and cellular resistance to Pt-based anti-cancer drugs. *EMBO Journal*, **34**(24), 2993–3008.

Qiu, Z., Dubin, A. E., Mathur, J., Tu, B., Reddy, K., Miraglia, L. J., Reinhardt, J., Orth, A. P., & Patapoutian, A. (2014). SWELL1, a plasma membrane protein, is an essential component of volume-regulated anion channel. *Cell*, **157**(2), 447–458.

Rehder, D. S., & Borges, C. R. (2010a). Cysteine sulfenic acid as an intermediate in disulfide bond formation and nonenzymatic protein folding. *Biochemistry*, **49**(35), 7748–7755.

Rehder, D. S., & Borges, C. R. (2010b). Possibilities and pitfalls in quantifying the extent of cysteine sulfenic acid modification of specific proteins within complex biofluids. *BMC Biochemistry*, **11**(1), 25.

Shimizu, T., Numata, T., & Okada, Y. (2004). A role of reactive oxygen species in apoptotic activation of volume-sensitive Cl^- channel. *Proceedings of the National Academy of Sciences, USA*, **101**(17), 6770–6773.

Stauber, T. (2015). The volume-regulated anion channel is formed by LRRC8 heteromers – molecular identification and roles in membrane transport and physiology. *Biological Chemistry*, **396**(9-10), 975–990.

Strange, K., Yamada, T., & Denton, J. S. (2019). A 30-year journey from volume-regulated anion currents to molecular structure of the LRRC8 channel. *Journal of General Physiology*, **151**(2), 100–117.

Tang, W., Ehrlich, I., Wolff, S. B., Michalski, A. M., Wolfl, S., Hasan, M. T., Luthi, A., & Sprengel, R. (2009). Faithful expression of multiple proteins via 2A-peptide self-processing: A versatile and reliable method for manipulating brain circuits. *Journal of Neuroscience*, **29**(27), 8621–8629.

Traverso, S., Zifarelli, G., Aiello, R., & Pusch, M. (2006). Proton sensing of CLC-0 mutant E166D. *Journal of General Physiology*, **127**(1), 51–66.

Varela, D., Simon, F., Olivero, P., Armisen, R., Leiva-Salcedo, E., Jorgensen, F., Sala, F., & Stutzin, A. (2007). Activation of H_2O_2-induced VSOR Cl^- currents in HTC cells require phospholipase Cgamma1 phosphorylation and Ca^{2+} mobilisation. *Cellular Physiology and Biochemistry*, **20**(6), 773–780.

Varela, D., Simon, F., Riveros, A., Jorgensen, F., & Stutzin, A. (2004). NAD(P)H oxidase-derived H(2)O(2) signals chloride channel activation in cell volume regulation and cell proliferation. *Journal of Biological Chemistry*, **279**(14), 13301–13304.

Voss, F. K., Ullrich, F., Munch, J., Lazarow, K., Lutter, D., Mah, N., Andrade-Navarro, M. A., von Kries, J. P., Stauber, T., & Jentsch, T. J. (2014). Identification of LRRC8 heteromers as an essential component of the volume-regulated anion channel VRAC. *Science*, **344**(6184), 634–638.

Zhou, C., Chen, X., Planells-Cases, R., Chu, J., Wang, L., Cao, L., Li, Z., Lopez-Cayuqueo, K. I., Xie, Y., Ye, S., Wang, X., Ullrich, F., Ma, S., Fang, Y., Zhang, X., Qian, Z., Liang, X., Cai, S. Q., Jiang, Z., … Xiao, H. (2020). Transfer of cGAMP into bystander cells via LRRC8 volume-regulated anion channels augments STING-mediated interferon responses and anti-viral immunity. *Immunity*, **52**(5), 767–781.e6.

Zhou, P., Polovitskaya, M. M., & Jentsch, T. J. (2018). LRRC8 N termini influence pore properties and gating of volume-regulated anion channels (VRACs). *Journal of Biological Chemistry*, **293**(35), 13440–13451.

Additional information

Data availability statement

All data generated or analysed during this study are included in the figures and tables.

Competing interests

The authors declare that they have no competing interests.

Author contributions

S.B., P.Z., P.G. and M.P. designed research; S.B. and M.P. performed research; S.B., P.Z., P.G. and M.P. analysed data; S.B. and M.P. wrote the paper. All authors have read and approved the final version of this manuscript and agree to be accountable for all aspects of the work in ensuring that questions related to the accuracy or integrity of any part of the work are appropriately investigated and resolved. All persons designated as authors qualify for authorship, and all those who qualify for authorship are listed.

Funding

This work was supported by a grant from the Fondazione AIRC per la Ricerca sul Cancro (grant no. IG 21558) and the Italian Research Ministry (PRIN 20174TB8KW) to M.P.

Acknowledgements

We thank Dr Francesca Quartino for expert technical assistance and Thomas Jentsch for the LRRC8 KO cells.

Open Access Funding provided by Consiglio Nazionale delle Ricerche within the CRUI-CARE Agreement.

Keywords

oxidation, start methionine, volume regulation, VRAC

Supporting information

Additional supporting information can be found online in the Supporting Information section at the end of the HTML view of the article. Supporting information files available:

Peer Review History
Statistical Summary Document